Amplitude control for an artificial hair cell undergoing an Andronov-Hopf bifurcation

Hermann Folke Johann Rolf * **Thomas Meurer** *

* Automation and Control Group, Faculty of Engineering, Kiel University, Kaiserstr. 2, D-24143 Kiel, Germany (e-mail: {foro, tm}@tf.uni-kiel.de).

Abstract: The dynamics of an artificial hair cell is analyzed by considering the bifurcation behavior of a dominant mode model. It is shown that this model undergoes an Andronov-Hopf bifurcation similar to its biological counterpart, i.e., the hair cell in the mammalian cochlea. Consequently, this dynamical behavior is exploited to control the amplitude of the deflection of the artificial hair cell. In particular feedforward control with disturbance injection is designed based on an approximation of the oscillation using an envelope model to achieve a constant deflection amplitude. The approach is evaluated in numerical simulations.

Keywords: Bifurcation analysis, Andronov-Hopf bifurcation, Envelope model, Amplitude control, Disturbance injection, Neuromorphic engineering

1. INTRODUCTION

Technological approaches in speech processing are divided into three different steps. These are detecting, preprocessing and analyzing the measured signal. Traditionally, the detection is done by a microphone with linear transfer function in the band from 20 Hz to 20 kHz and a noise floor of 20-30 dB (Zawawi et al., 2020). However, the desired signal can be jammed by background noises. Due to this, it is difficult to use speech processing in conditions with many interfering sources. To circumvent this crucial problem it can be helpful to to imitate a biological approach, i.e., the active sound sensing of the mammalian ear (Gold et al., 1948; Gold and Gray, 1948). On the one hand the mammalian ear is capable to detect and process the incoming sound waves so that it can recover heavily distorted signals simultaneously. This is called cocktail party effect. On the other hand, the ear has a high dynamical range in detecting sounds. These properties are assumed to be achieved by the remarkable dynamical behavior of the hair cells in the cochlea. The hair cell is believed to exhibit an Andronov-Hopf bifurcation (Camalet et al., 2000; Eguíluz et al., 2000), which emerges from a feedback loop changing the stiffness of the hair cell. This feedback loop is activated by the change of the pressure opening and closing the mechanoelectrical transduction (MET) channels (Fettiplace and Hackney, 2006).

For the transfer of these concepts to a technical device imitating the hair cell Lenk et al. (2018, 2020) use a micromechanical beam. In the following this system is summarized: The beam has a characteristic frequency between 20 Hz and 20 kHz so that the length of this beam is in the range of 100 micrometers. Moreover, a non-linearity is introduced by actively heating the beam using a voltage-controlled thermal actuator (Roeser et al., 2016). It has been shown that the beam has three different operation modes under velocity feedback. The system is in the passive (first) mode, if the feedback strength is chosen to be close to zero. After increasing the feedback strength it enters the active mode, where the beam's sensitivity to sound pressure i enhanced. Having passed another threshold, the beam enters a mode of sustained autonomous oscillations. Based on the different operations modes, it is assumed that the thermally actuated beam exhibits at least one Andronov-Hopf bifurcation (Lenk et al., 2018, 2020). This beam is subsequently referred to as artificial hair cell.

Usually an Andronov-Hopf bifurcation is used to show, that a limit cycle emerges in a high dimensional system once a bifurcation parameter exceeds a certain threshold. In contrast, if this threshold is is not exceeded by the bifurcation parameter, the system will be asymptotically stable (Marsden and McCracken, 1976). Thus, this stable regime is called sub-threshold regime. In this regime the system exhibiting an Andronov-Hopf bifurcation has two advantageous properties. At first a compressive non-linearity can be observed so that incoming signals are amplified depending on their amplitude, i.e., the smaller an amplitude the stronger the amplification. In particular, the gain at the bifurcation point is infinitely large for a signal with amplitude close to zero. Secondly, these systems are very frequency selective (Camalet et al., 2000; Eguíluz et al., 2000; Duke and Jülicher, 2007).

In this paper the bifurcation analysis of the artificial hair cell is performed eventually leading to the design of a feedforward controller with disturbance injection, which exploits an Andronov-Hopf bifurcation to control the beam's deflection amplitude. Consequently, this amplitude controller uses the amplification of the beam to encode the external input in the feedback strength. For this, the dominating mode model of the hair cell is introduced in Section

2 followed by its bifurcation analysis. In Section 3 the amplitude controller is designed to assign a constant value for the deflection amplitude based on the knowledge of the external input and the properties of the Andronov-Hopf bifurcation in the sub-threshold regime. Control design is based on an envelope model of the artificial hair cell. The results are evaluated numerically in Section 4. Some final remarks conclude the paper.

2. BIFURCATION ANALYSIS

In the following, the artificial hair cell is assumed to be represented by a dominant (single) mode approximation of a thermally actuated flexible micromechanical beam, see Roeser et al. (2016) for the derivation of the respective distributed parameter model and the modal reduction [2]. In particular, the coupled system of ordinary differential equations (ODEs) is considered

$$\dot{\boldsymbol{x}} = \begin{bmatrix} x_2 \\ -\omega_0^2 x_1 - \frac{\omega_0}{Q_0} x_2 + \alpha x_3 + F_{\text{ext}} \\ -\beta x_3 + \frac{\gamma}{R^2} u_{\text{act}}^2 \end{bmatrix}, \ t > 0, \ \boldsymbol{x}(0) = \boldsymbol{x}_0 \quad (1a)$$

$$y = x_1, \quad t \geq 0. \quad (1b)$$

Herein the state vector $\boldsymbol{x}(t) = [x_1(t), x_2(t), x_3(t)]^{\text{T}} \in \mathbb{R}^3$ is composed of deflection, velocity, and relative temperature, respectively, with $y(t)$ denoting the measured output. Parameters are given by the characteristic frequency $\omega_0 > 0$, the Q-factor $Q_0 > 0$, the transfer factors $\alpha, \gamma > 0$, the time constant $\beta > 0$, and the heater resistance $R > 0$. The controllable (thermal) input is given by $u_{\text{act}}(t) \in \mathbb{R}$ and $F_{\text{ext}}(t) \in \mathbb{R}$ denotes an external force. Note that the model of the cantilever is linear, if $u_{\text{act}} = 0$. To impose an Andronov-Hopf bifurcation and hence to achieve a behavior similar to a real hair cell, u_{act} must be assigned accordingly. For this and in view of a practical realization the measured deflection $y(t)$ is high pass filtered using $G_{\text{HP}}(s) = k\tau s / (1 + \tau s)$ with the time constant $\tau > 0$ and the calibration factor $k \in \mathbb{R}$. Taking into account (1) the effect of the high pass filter can be addressed in terms of the additional state $x_4(t)$ given

$$\dot{x}_4 = -\frac{1}{\tau} x_4 + k x_2, \quad t > 0, \ x_4(0) = x_{4,0}. \quad (2)$$

Substituting the proportional feedback $u_{\text{act}} = a x_4 + u_{\text{DC}}$ with gain $a \in \mathbb{R}$ and DC-voltage $u_{\text{DC}} \in \mathbb{R}$ into (1) and amending (2) yields the extended system

$$\dot{\boldsymbol{x}} = \underbrace{\begin{bmatrix} x_2 \\ -\omega_0^2 x_1 - \frac{\omega_0}{Q_0} x_2 + \alpha x_3 + F_{\text{ext}} \\ -\beta x_3 + \frac{\gamma}{R^2} (a x_4 + u_{\text{DC}})^2 \\ -\frac{1}{\tau} x_4 + k x_2 \end{bmatrix}}_{= \boldsymbol{f}(\boldsymbol{x})}, \ t > 0, \ \boldsymbol{x}(0) = \boldsymbol{x}_0 \quad (3a)$$

$$y = x_1, \quad t \geq 0. \quad (3b)$$

To determine the principle bifurcation points the eigenvalues of the linearization of (3) at its equilibria are analyzed. An equilibrium $\boldsymbol{x}_e$ are thereby determined by solving $\boldsymbol{f}(\boldsymbol{x}_e) = \boldsymbol{0}$, which yields

---

[2] The mechanical subsystem of the beam is modeled as a Euler-Bernoulli beam with the Duhamel-Neumann law and the thermal subsystem is modeled as a Fourier heat conduction.

$$\boldsymbol{x}_{\text{e}} = \begin{bmatrix} \frac{\alpha\gamma}{\beta\omega_0^2 R^2} u_{\text{DC}}^2 & 0 & \frac{\gamma}{\beta R^2} u_{\text{DC}}^2 & 0 \end{bmatrix}^{\text{T}}. \quad (4)$$

Obviously, changing u_{DC} allows to adjust the equilibrium value. Let $\Delta \boldsymbol{x} = \boldsymbol{x} - \boldsymbol{x}_{\text{e}}$ denote the distance to $\boldsymbol{x}_{\text{e}}$. Then making use of the Taylor series expansion implies

$$\Delta \dot{\boldsymbol{x}} = A_{\text{lin}} \Delta \boldsymbol{x}, \quad t > 0, \ \Delta \boldsymbol{x}_e(0) = \Delta \boldsymbol{x}_{e,0} \quad (5a)$$

with the Jacobian matrix

$$A_{\text{lin}} = \frac{\partial \boldsymbol{f}(\boldsymbol{x})}{\partial \boldsymbol{x}}\bigg|_{\boldsymbol{x}=\boldsymbol{x}_e} = \begin{bmatrix} 0 & 1 & 0 & 0 \\ -\omega_0^2 & -\frac{\omega_0}{Q_0} & \alpha & 0 \\ 0 & 0 & -\beta & \frac{2\gamma a u_{\text{DC}}}{R^2} \\ 0 & k & 0 & -\frac{1}{\tau} \end{bmatrix}. \quad (5b)$$

With these preparations the following result can be formulated.

Theorem 1. The system (3) undergoes two Andronov-Hopf bifurcations depending on the feedback gain a with the bifurcation points given by (A.1a). The resonance frequencies ω_{R} of the Andronov-Hopf bifurcations are given by (A.1b).

Proof. The proof is based on Hopf's Theorem in $\mathbb{R}^n$, see, e.g., Marsden and McCracken (1976), and follows two steps: First it is shown that A_{lin} defined in (5) has at least one pair of complex conjugated eigenvalues with zero real part. With this the bifurcation point is derived. Secondly, it is shown that the remaining spectrum remains in the left half complex plane, while the complex conjugated eigenvalues are crossing the imaginary axis. By showing this, it is proven that the bifurcation at that point is indeed an Andronov-Hopf bifurcation.

To proof the first part, consider the characteristic polynomial of the system matrix A_{lin}, which is given by

$$p(\lambda) = \lambda^4 + \left(\frac{1}{\tau} + \beta + \frac{\omega_0}{Q_0}\right)\lambda^3 + \left(\frac{\beta}{\tau} + \omega_0^2 + \frac{\omega_0}{Q_0\tau} + \frac{\beta\omega_0}{Q_0}\right)\lambda^2$$
$$+ \left(\beta\omega_0^2 + \frac{\omega_0^2}{\tau} + \frac{\beta\omega_0}{Q_0\tau} - \frac{2\alpha a\gamma k u_{\text{DC}}}{R^2}\right)\lambda + \frac{\beta\omega_0^2}{\tau}. \quad (6)$$

To verify that two roots are crossing the imaginary axis at a_{crit} consider the general form of a polynomial with two roots having zero real part, i.e.,

$$p_{a_{\text{crit}}}(\lambda) = \left(\lambda^2 + s_0 \lambda + s_1\right)\left(\lambda^2 + \omega_{\text{R}}^2\right)$$
$$= \lambda^4 + s_0 \lambda^3 + \left(s_1 + \omega_{\text{R}}^2\right)\lambda^2 + s_0\omega_{\text{R}}^2\lambda + s_1\omega_{\text{R}}^2$$

with $s_0, s_1 \in \mathbb{R}$ and resonance frequency $\omega_{\text{R}} \in \mathbb{R}$. By comparing the coefficients of the polynomial $p(\lambda)$ and $p_{a_{\text{crit}}}(\lambda)$, the bifurcation point a_{crit} and the resonance frequency ω_{R} can be directly determined in the form (A.1a) and (A.1b), respectively.

To show that only one pair of complex conjugated eigenvalues crosses the imaginary axis, the remaining eigenvalues of (6) have to stay in the left half complex plane. This can be proven by showing that the coefficients s_0 and s_1 are positive, since then the polynomial $\lambda^2 + s_0 \lambda + s_1$ is a Hurwitz polynomial. The coefficients are given by

$$s_0 = \frac{1}{\tau} + \beta + \frac{\omega_0}{Q_0}, \quad s_1 = \frac{\beta}{\tau} + \omega_0^2 + \frac{\omega_0}{Q_0\tau} + \frac{\beta\omega_0}{Q_0} - \omega_{\text{R}}^2.$$

Obviously, $s_0 > 0$ holds true, since all parameters (except u_{DC}) are defined to be positive. Moreover, (A.1b) satisfies

$$\omega_{\text{R}}^2 < \frac{\beta}{\tau} + \omega_0^2 + \frac{\omega_0}{Q_0\tau} + \frac{\beta\omega_0}{Q_0},$$

since the inner square root can be bounded by

$$\sqrt{(\omega_0(\beta\tau + 1) + Q_0\,(\beta + \tau\omega_0^2))^2 - 4\beta Q_0^2 \tau\omega_0^2}$$
$$< \omega_0(\beta\tau + 1) + Q_0\,(\beta + \tau\omega_0^2).$$

Hence, it can be concluded that s_1 is also positive, because all parameters (except u_{DC}) are positive so that the polynomial $\lambda^2 + s_0\lambda + s_1$ is a Hurwitz polynomial. This concludes the proof. $\square$

Remark 2. According to Hopf's Theorem the limit cycle is attractive, if the equilibrium is asymptotically stable at the bifurcation points. Numerical results indicate that (3) is not asymptotically stable at the bifurcation points a_{crit}. An analytical verification of this observation, which is outside the scope of this paper, might be based on the Center Manifold Theorem applied to the system

$$\dot{\boldsymbol{z}} = A_{\text{lin}}\boldsymbol{z} + \frac{\gamma a^2}{R^2}\begin{bmatrix} 0 \\ 0 \\ z_4^2 \\ 0 \end{bmatrix}.$$

in the state $\boldsymbol{z} = \boldsymbol{x} - \boldsymbol{x}_e$ with $\boldsymbol{x}_e$ from (4). As by definition the eigenvalues of A_{lin} are form by a pair of conjugated complex eigenvalues with zero real part and two eigenvalues with negative part it is necessary to take into account the additive nonlinear perturbation for the stability assessment.

3. ENVELOPE MODEL AND AMPLITUDE CONTROL BY DISTURBANCE INJECTION

Subsequently an amplitude controller composed of a feed-forward controller with distortion injection $t \mapsto a_{DI}(t)$ to adjust the feedback gain parameter a in (3) is determined based on an envelope model. With this the amplitude of the output $y = x_1$ of (3) is supposed to maintain a constant prescribed value under external excitation. By exploiting the dynamical range of an Andronov-Hopf bifurcation this allows to encode the information of the external input F_{ext} in the temporal evolution of the feedback strength a_{DI} so that the artificial hair cell adapts its sensitivity and uses the amplification induced by the Andronov-Hopf bifurcation effectively.

3.1 Determination of the envelope model

Envelope models in general were developed in, e.g., Sanders and Noworolski (1991); Sanders et al. (1991); Caliskan et al. (1999). They are in principle based on the derivation of ODEs describing the temporal evolution of Fourier coefficients of the trajectory. In view of controlling the oscillation amplitude, this approach allows to reduce the computational burden as larger sampling times can be used compared to those necessary to resolve rather high frequency oscillations. Following Egretzberger and Kugi (2010); Egretzberger et al. (2012), consider the ansatz

$$x_i = q_{i,0} + q_{i,1}\cos(\omega_s t) + q_{i,2}\sin(\omega_s t) \qquad (7)$$

with the Fourier coefficients $q_{i,j}(t) \in \mathbb{R}$, $j \in \{0, 1, 2\}$ for the state $x_i(t)$, $i \in \{1, ..., 4\}$ and the sampling frequency $\omega_s > 0$. As system (3) exhibits an Andronov-Hopf bifurcation, the envelope model is expected to be very sensitive to a change of the sampling frequency ω_s around the bifurcation point(s). Therefore, it is crucial to analyze the behavior of the envelope model in view of the choice of ω_s.

The temporal evolution of the Fourier coefficients $q_{i,j}(t)$ can be determined from (3) by substituting

$$\dot{x}_i = \dot{q}_{i,0} + (\dot{q}_{i,1} + \omega_s q_{i,2})\cos(\omega_s t)$$
$$+ (\dot{q}_{i,2} - \omega_s q_{i,1})\sin(\omega_s t) \quad (8)$$

and (7). Thereby

$$(x_4)^2 = (q_{4,0} + q_{4,1}\cos(\omega_s t) + q_{4,2}\sin(\omega_s t))^2$$
$$\approx q_{4,0}^2 + 2q_{4,0}[q_{4,1}\cos(\omega_s t) + q_{4,2}\sin(\omega_s t)] \qquad (9)$$

is used in view of (7), which results in the envelope model

$$\frac{d}{dt}\begin{bmatrix} q_{1,0} \\ q_{1,1} \\ q_{1,2} \\ q_{2,0} \\ q_{2,1} \\ q_{2,2} \\ q_{3,0} \\ q_{3,1} \\ q_{3,2} \\ q_{4,0} \\ q_{4,1} \\ q_{4,2} \end{bmatrix} = \begin{bmatrix} q_{2,0} \\ -\omega_s q_{1,2} + q_{2,1} \\ \omega_s q_{1,1} + q_{2,2} \\ -\omega_0^2 q_{1,0} - \frac{\omega_0}{Q_0}q_{2,0} + \alpha q_{3,0} + \frac{1}{m}f_{\text{ext},0} \\ -\omega_0^2 q_{1,1} - \frac{\omega_0}{Q_0}q_{2,1} - \omega_s q_{2,2} + \alpha q_{3,1} + \frac{1}{m}f_{\text{ext},1} \\ -\omega_0^2 q_{1,2} - \frac{\omega_0}{Q_0}q_{2,2} + \omega_s q_{2,1} + \alpha q_{3,2} + \frac{1}{m}f_{\text{ext},2} \\ -\beta q_{3,0} + \frac{2du_{DC}}{a}q_{4,0} + h(\boldsymbol{q}_4) + \frac{u_{DC}^2\gamma}{R^2} \\ -\beta q_{3,1} - \omega_s q_{3,2} + \frac{2du_{DC}}{a}q_{4,1} + 2dq_{4,0}q_{4,1} \\ -\beta q_{3,2} + \omega_s q_{3,1} + \frac{2du_{DC}}{a}q_{4,2} - 2dq_{4,0}q_{4,2} \\ -\frac{1}{\tau}q_{4,0} + kq_{2,0} \\ -\frac{1}{\tau}q_{4,1} - \omega_s q_{4,2} + kq_{2,1} \\ \omega_s q_{4,1} - \frac{1}{\tau}q_{4,2} + kq_{2,2} \end{bmatrix}. \qquad (10)$$

Herein, $d = a^2\gamma/R^2$, $h(\boldsymbol{q}_4) = d(q_{4,0}^2 + [q_{4,1}^2 + q_{4,2}^2]/2)$ and the Fourier coefficients of the external input F_{ext} are denoted by $f_{\text{ext},j}(t) \in \mathbb{R}$, $j \in \{0, 1, 2\}$.

3.2 Feedforward control with disturbance injection

In the following, the amplitude controller for the two Fourier coefficients $q_{1,1}$ and $q_{1,2}$ describing the harmonic contributions in the output signal $y = x_1$ is designed. For this, it is assumed that the Fourier coefficients $f_{\text{ext},j}(t)$ of the external input F_{ext} are known and thus can be injected by means of the amplitude controller. After that, the gain of an artificial hair cell is derived, i.e., the change of the amplitude of the output compared to the amplitude of the external input. The design is structured as follows: First, the equilibria of (10) are derived. With this, the amplitude of both Fourier coefficients of the equilibria $q_{1,j,e}$ is determined by

$$A = \sqrt{q_{1,1,e}^2 + q_{1,2,e}^2}. \qquad (11)$$

This equation establishes a relationship between the amplitude A, the external input F_{ext}, and the feedback strength a. Interestingly, the system of equations to derive the equilibria of (10) can be decoupled, because $q_{4,0,e}$ vanishes, such that two linear equation system emerge. The solution of these equations is summarized in (A.2). To determine the amplitude A insert (A.2) into (11). After simplification this results in

$$A = \frac{\sqrt{f_2^2 + f_3^2}\, Q_0 R^2 \sqrt{\beta^2 + \omega_s^2}\sqrt{\tau^2\omega_s^2 + 1}}{m\sqrt{K(a)}}. \qquad (12)$$

with $K(a)$ given by (A.2d). Secondly, (12) has to be solved for $a = a_{DI}$ to derive the feedforward controller with disturbance injection. This yields (A.3). Last, the gain can be derived by substituting (12) into

$$G = \frac{A}{\sqrt{f_{\text{ext},1}^2 + f_{\text{ext},2}^2}} \qquad (13)$$

(a) Maximum gain $G_{\max}$ of the artificial hair cell in terms of the sampling frequency ω_s.

(b) Gain G of the artificial hair cell in terms of feedback parameter a and the sampling frequency ω_s.
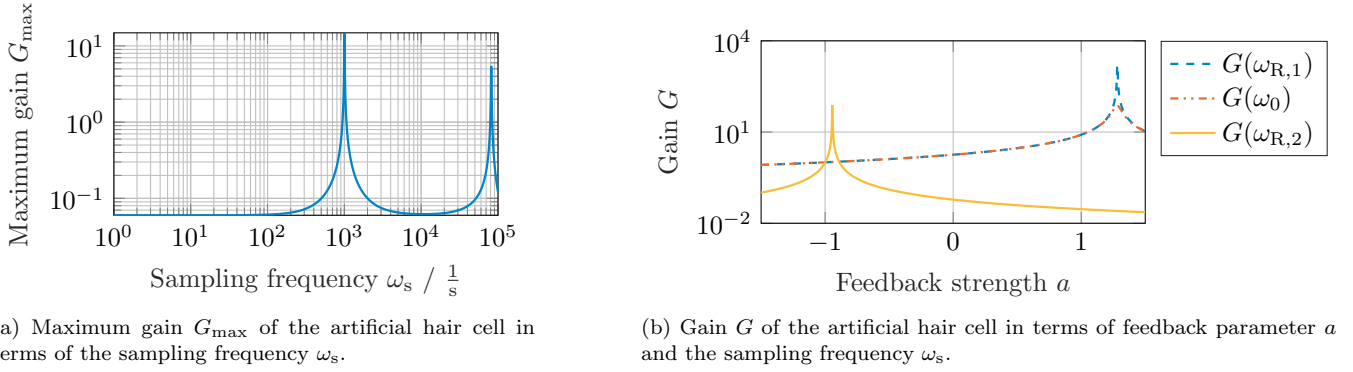
Fig. 1. Gain response of the artificial hair in terms of the sampling frequency ω_s and the feedback strength a.

and the maximum gain can be determined by setting the square root of (A.3) to zero as

$$G_{\max} = \frac{Q_0\sqrt{(\beta^2 + \omega_s^2)(\tau^2\omega_s^2 + 1)}}{m\left|Q_0\left(\omega_0^2 - \omega_s^2\right)\left(\tau\omega_s^2 - \beta\right) + (\beta\tau + 1)\omega_0\omega_s^2\right|} \quad (14)$$

4. NUMERICAL RESULTS

To conclude this paper, the amplitude controller a_{DI} is evaluated numerically. For this the parameters are chosen according to Table 1. With these parameters the critical feedback strengths from (A.1a) read $a_{\mathrm{crit},1} = 1.2823$ and $a_{\mathrm{crit},2} = -0.9437$. Furthermore, (A.1b) yields the resonance frequencies $\omega_{\mathrm{R},1} = 2\pi \times 13005.3$ Hz and $\omega_{\mathrm{R},2} = 2\pi \times 159.61$ Hz.

At first, the gain $G(a, \omega_s)$ and the maximum gain $G_{\max}(\omega_s)$ from (13) and (14) are computed. The result is depicted in Figure 1. The maximum gain $G_{\max}$ in terms of the sampling frequency ω_s is shown in Figure 1a. It can be seen that it is maximized at the resonance frequencies $\omega_{\mathrm{R},1}$ and $\omega_{\mathrm{R},2}$. Additionally, the frequency selectivity of the respective Andronov-Hopf bifurcations is shown, since a small deviation from the resonance frequencies $\omega_{\mathrm{R},1}$ and $\omega_{\mathrm{R},2}$ results in a drastic decrease of the maximum gain $G_{\max}$. The gain $G(a, \omega_s)$ in terms of the feedback parameter a is shown in Figure 1b. For this, the sampling frequencies is chosen as $\omega_s \in \{\omega_{\mathrm{R},1}, \omega_0, \omega_{\mathrm{R},2}\}$. It can be seen that as the sampling frequency ω_s changes from $\omega_{\mathrm{R},1}$ to $\omega_{\mathrm{R},2}$, the bifurcation point a_{crit} moves from $a_{\mathrm{crit},1}$ to $a_{\mathrm{crit},2}$.

Secondly, (3) and (10) are solved numerically and compared to each other. Especially, note that the sampling frequency is chosen to be $\omega_s = \omega_0$ and that the maximum gain with this configuration is $G_{\max} = 732.3$ s/kg. Again, this shows the frequency selectivity of the Andronov-Hopf bifurcation, since the difference of the frequencies is $\omega_\Delta = 2\pi \times 0.5$. Moreover, the envelope of the deflection is approximated using

$$\tilde{x}_1(t) \approx q_{1,0}(t) + \sqrt{q_{1,1}(t)^2 + q_{1,2}(t)^2}.$$

and the a time-dependent external force $F_{\mathrm{ext}}(t)$ is defined in terms of its Fourier coefficients

$f_{\mathrm{ext},0} = 0,$

$$f_{\mathrm{ext},1} = \begin{cases} \hat{f}_{\mathrm{ext},1}, & \text{if } t \leq t_1, \\ \hat{f}_{\mathrm{ext},1} - (\hat{f}_{\mathrm{ext},1} - \hat{f}_{\mathrm{ext},2})\dfrac{t - t_1}{t_2 - t_1}, & \text{if } t \in (t_1, t_2], \\ \hat{f}_{\mathrm{ext},2}, & \text{if } t \in (t_3, t_4), \\ \hat{f}_{\mathrm{ext},2} + (\hat{f}_{\mathrm{ext}3} - \hat{f}_{\mathrm{ext}2})\dfrac{t - t_2}{t_3 - t_2}, & \text{if } t \in [t_4, t_5), \\ [1 + 0.25\sin(2\pi t)]\,\hat{f}_{\mathrm{ext},3}, & \text{if } t \geq t_5, \end{cases}$$

$f_{\mathrm{ext},2} = 0$

with amplitudes $\hat{f}_{\mathrm{ext},1} = 18 \times 10^{-9}$ kgm/s, $\hat{f}_{\mathrm{ext},2} = 1.25 \times 10^{-9}$ kgm/s, $\hat{f}_{\mathrm{ext},3} = 8 \cdot 10^{-9}$ kgm/s, and the time instances $t_k = 3k$ s, $k \in \{1, ..., 5\}$. The simulation results are shown in Figure 2. The deflection x_1 is depicted in Figure 2a. Obviously the approximation of the envelope $\tilde{x}_1$ estimating the temporal evolution of the envelope of deflection x_1 is well in the non-grey shaded areas. This result from the fact that the feedback strength a is small such that the influence of the non-linearity is weak. However, if the feedback strengths a is increased, the estimation $\tilde{x}_1$ becomes invalid. In this case, higher modes induced by the non-linearity x_4^2 become more dominant. This is shown in the gray-shaded area of Figure 2a. Moreover, the evolution of the first mode of the external input $f_{\mathrm{ext},1}$ is shown in Figure 2b and the evolution of the amplitude controller a_{DI} and its bounds $a_{\mathrm{crit},1}$ and $a_{\mathrm{crit},2}$ are depicted in Figure 2c. As expected, the feedback gain a is close to the upper bound for $t \in [t_3, t_4]$. This is due to the small amplitude of $f_{\mathrm{ext},1}$. Additionally, the evolution of the envelope A with and without the amplitude controller is shown in Figure 2d. Note that the amplitude of the artificial hair cell with amplitude controller and with constant feedback strength are denoted by A_{DI} and A_{c}, respectively. The amplitude controller with disturbance injection a_{DI} keeps the envelope of A_{DI} approximately constant.

5. CONCLUSION

Given the dominant mode model in terms of a thermally actuated micromechanical beam representing an artificial hair cell a nonlinear feedforward control with disturbance injection is developed for keeping the oscillation envelope constant under external excitation. For this, the bifurcations of the artificial hair cell are analyzed. In particular it is shown that the used model exhibits two Andronov-Hopf bifurcations. The amplitude controller is designed based on a truncated envelope model. The truncation is valid
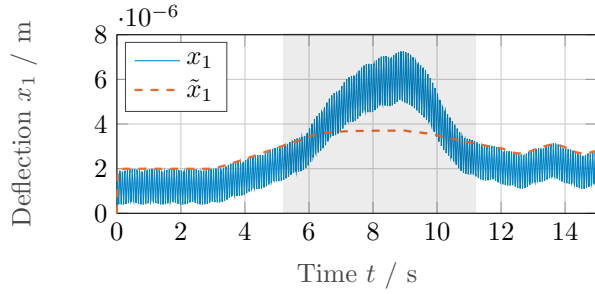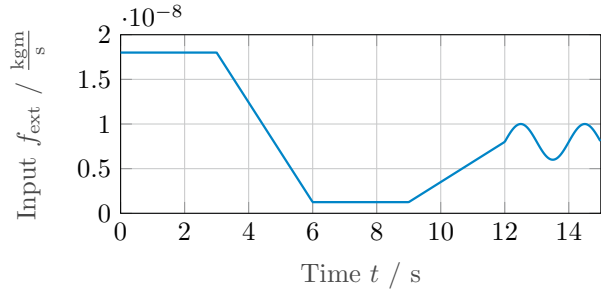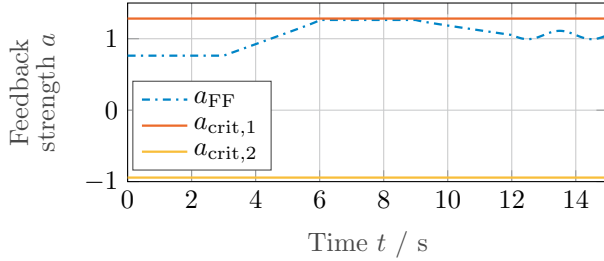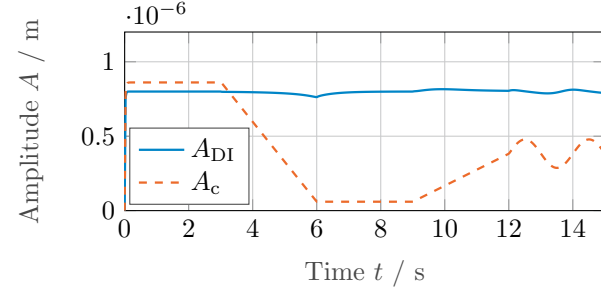
(a) Evolution of the trajectory x_1 and the approximated envelope $\tilde{x}_1$.

(b) Evolution of the Fourier coefficient $f_{\text{ext},1}$ of the external input F_{ext}.

(c) Evolution of the a_{DI}. The critical feedback strengths $a_{\text{crit},1}$ and $a_{\text{crit},2}$ indicate the limitations of a_{DI}.

(d) Evolution of the amplitude A_{DI} with the amplitude controller and the amplitude A_{c} with constant feedback strength a_{c}.

Fig. 2. Numerical solution of (3) and (10) with the amplitude controller a_{DI} from (A.3) and the constant feedback strength a_{C}.

Table 1. Parameters of the simulation

Parameter	Value
Resonance frequency ω_0	$2\pi \times 13$ kHz
Sampling frequency ω_{s}	$2\pi \times 13$ kHz
Q-Factor Q_0	30
Offset voltage u_{DC}	-0.2 V
Transfer factor γ	4.2588×10^7
Transfer factor α	$749.3702 \frac{\text{m}}{\text{Ks}}$
Time constant β	$1006.6 \frac{1}{\text{s}}$
Time constant τ	$10^{-3} \frac{1}{\text{s}}$
Resistance of the heater R	$30 \ \Omega$
Calibration factor k	$10^6 \frac{\text{V}}{\text{m}}$
Constant feedback strength a_{c}	0.8
Mass m	2.5×10^{-10} kg
Desired amplitude A^*	0.8×10^{-8} m

as an Andronov-Hopf bifurcation is frequency selective. Additionally, an analytical expression for the gain, i.e., the relative change of the amplitude of the artificial hair cell with respect to the amplitude of the excitation signal is derived to show the remarkable dynamical range of an Andronov-Hopf bifurcation. Simulation results illustrate the performance of this concept.

ACKNOWLEDGEMENTS

Appendix A. EQUATIONS

The equations for the bifurcation point, resonance frequency, equilibria of the envelope model, and the feedforward controller with distortion injections are summarized in (A.1a), (A.1b), (A.2), and (A.3), respectively.

REFERENCES

Caliskan, V., Verghese, O., and Stankovic, A. (1999). Multifrequency averaging of DC/DC converters. *IEEE Transactions on Power Electronics*, 14(1), 124–133. Conference Name: IEEE Transactions on Power Electronics.

Camalet, S., Duke, T., Julicher, F., and Prost, J. (2000). Auditory sensitivity provided by self-tuned critical oscillations of hair cells. *Proceedings of the National Academy of Sciences*, 97(7), 3183–3188.

Duke, T.A. and Jülicher, F. (2007). Critical Oscillators as Active Elements in Hearing. In G.A. Manley, R.R. Fay, and A.N. Popper (eds.), *Active Processes and Otoacoustic Emissions in Hearing*, volume 30, 63–92. Springer New York, New York, NY. Series Title: Springer Handbook of Auditory Research.

Egretzberger, M. and Kugi, A. (2010). A dynamical envelope model for vibratory gyroscopes. *Microsystem Technologies*, 16(5), 777–786.

Egretzberger, M., Mair, F., and Kugi, A. (2012). Model-based control concepts for vibratory MEMS gyroscopes. *Mechatronics*, 22(3), 241–250.

Eguíluz, V.M., Ospeck, M., Choe, Y., Hudspeth, A.J., and Magnasco, M.O. (2000). Essential Nonlinearities in Hearing. *Physical Review Letters*, 84(22), 5232–5235. Publisher: American Physical Society.

Fettiplace, R. and Hackney, C.M. (2006). The sensory and motor roles of auditory hair cells. *Nature Reviews Neuroscience*, 7(1), 19–29.

Gold, T. and Gray, J. (1948). Hearing. II. The physical basis of the action of the cochlea. *Proceedings of the Royal Society B: Biological Sciences*, 135(881), 492–498.

Gold, T., Pumphrey, R.J., and Gray, J. (1948). Hearing. I. The cochlea as a frequency analyzer. *Proceedings of the*

Bifurcation point and resonance frequency of the artificial hair cell

$$
a_{\text{crit}} = \frac{-R^2}{4\gamma\alpha\tau^2 k u_{\text{DC}}} \left[\left(\beta + \beta^2\tau + \frac{\omega_0}{Q_0}\left(1 + \beta\tau + \beta^2\tau^2\right) + \frac{\omega_0^2}{Q_0}\left(\frac{1}{Q_0} - Q\right)\left(\tau + \beta\tau^2\right) + \frac{\omega_0^3}{Q_0}\tau^2 \right) \right.
$$
$$
\left. \pm \left(1 + \beta\tau + \frac{\tau\omega_0}{Q_0}\right)\sqrt{\left(\frac{\omega_0}{Q_0} + \tau\omega_0^2\right)^2 + \left(\beta + \beta\tau\frac{\omega_0}{Q_0}\right)^2 + 2\beta\omega_0\left(\frac{1}{Q_0} + \frac{\tau\omega_0}{Q_0^2} + \frac{\tau^2\omega_0^2}{Q_0} - \tau\omega_0\right)} \right]. \tag{A.1a}
$$

$$
\omega_{\text{R}} = \sqrt{\frac{\beta\tau\omega_0 + \beta Q_0 + Q_0\tau\omega_0^2 + \omega_0 \pm \sqrt{\left(\omega_0(\beta\tau+1) + Q_0\left(\beta + \tau\omega_0^2\right)\right)^2 - 4\beta Q_0^2\tau\omega_0^2}}{2Q_0\tau}} \tag{A.1b}
$$

Equilibria of the envelope model

$$
q_{1,0,\text{e}} = \frac{\alpha\gamma m\left(a^2\left(q_{1,1,\text{e}}^2 + q_{1,2,\text{e}}^2\right) + u_{\text{DC}}^2\right) + \beta R^2 f_{\text{ext},0}}{\beta m R^2\omega_0^2} \tag{A.2a}
$$

$$
q_{1,1,\text{e}} = \frac{Q_0^2 R^2\left(R^2\omega_0^2\left(\beta^2 + \omega_{\text{s}}^2\right)\left(\tau^2\omega_{\text{s}}^2 + 1\right) - \omega_{\text{s}}^2\left(2a\alpha\gamma k\tau(\beta\tau + 1)u_{\text{DC}} + R^2\left(\beta^2 + \omega_{\text{s}}^2\right)\left(\tau^2\omega_{\text{s}}^2 + 1\right)\right)\right)f_{\text{ext},2}}{mK(a)}
$$
$$
- \frac{Q_0 R^2\omega_{\text{s}}\left(2a\alpha\gamma k Q_0\tau u_{\text{DC}}\left(\tau\omega_{\text{s}}^2 - \beta\right) + R^2\omega_0\left(\beta^2 + \omega_{\text{s}}^2\right)\left(\tau^2\omega_{\text{s}}^2 + 1\right)\right)f_{\text{ext},2}}{mK(a)} \tag{A.2b}
$$

$$
q_{1,1,\text{e}} = \frac{Q_0 R^2\omega_{\text{s}}\left(2a\alpha\gamma k Q_0\tau u_{\text{DC}}\left(\tau\omega_{\text{s}}^2 - \beta\right) + R^2\omega_0\left(\beta^2 + \omega_{\text{s}}^2\right)\left(\tau^2\omega_{\text{s}}^2 + 1\right)\right)f_{\text{ext},1}}{mK(a)}
$$
$$
+ \frac{Q_0^2 R^2\left(R^2\omega_0^2\left(\beta^2 + \omega_{\text{s}}^2\right)\left(\tau^2\omega_{\text{s}}^2 + 1\right) - \omega_{\text{s}}^2\left(2a\alpha\gamma k\tau(\beta\tau + 1)u_{\text{DC}} + R^2\left(\beta^2 + \omega_{\text{s}}^2\right)\left(\tau^2\omega_{\text{s}}^2 + 1\right)\right)\right)f_{\text{ext},2}}{mK(a)} \tag{A.2c}
$$

$$
K(a) = Q_0^2\left(4a^2\alpha^2\gamma^2 k^2\tau^2 u_{\text{DC}}^2\omega_{\text{s}}^2 + R^2\left(\omega_0^2 - \omega_{\text{s}}^2\right)\left(R^2\omega_0^2\left(\beta^2 + \omega_{\text{s}}^2\right)\left(\tau^2\omega_{\text{s}}^2 + 1\right)\right.\right.
$$
$$
\left.\left. - \omega_{\text{s}}^2\left(4a\alpha\gamma k\tau(\beta\tau + 1)u_{\text{DC}} + R^2\left(\beta^2 + \omega_{\text{s}}^2\right)\left(\tau^2\omega_{\text{s}}^2 + 1\right)\right)\right)\right)
$$
$$
+ 4a\alpha\gamma k Q_0 R^2\tau\omega_0 u_{\text{DC}}\omega_{\text{s}}^2\left(\tau\omega_{\text{s}}^2 - \beta\right) + R^4\omega_0^2\omega_{\text{s}}^2\left(\beta^2 + \omega_{\text{s}}^2\right)\left(\tau^2\omega_{\text{s}}^2 + 1\right) \tag{A.2d}
$$

Feedforward controller with disturbance injections

$$
a_{\text{DI}} = \frac{R^2\omega_0\left(\beta + Q_0\omega_0(\beta\tau + 1)\right) - \omega_{\text{s}}^2\left(Q_0(\beta\tau + 1) + \tau\omega_0\right)}{2\alpha\gamma k Q_0\tau u_{\text{DC}}}
$$
$$
- \frac{R^2\sqrt{Q_0^2\left(\beta^2 + \omega_{\text{s}}^2\right)\left(\tau^2\omega_{\text{s}}^2 + 1\right)\left(f_{\text{ext},1}^2 + f_{\text{ext},2}^2\right) - A^2 m^2\left(Q_0\left(\omega_0^2 - \omega_{\text{s}}^2\right)\left(\tau\omega_{\text{s}}^2 - \beta\right) + \omega_0(\beta\tau + 1)\omega_{\text{s}}^2\right)^2}}{2\alpha\gamma k Q_0\tau u_{\text{DC}} m\omega_{\text{s}} A} \tag{A.3}
$$

Royal Society B: Biological Sciences, 135(881), 462–491.

Lenk, C., Ekinci, A., Rangelow, I.W., and Gutschmidt, S. (2018). Active, artificial hair cells for biomimetic sound detection based on active cantilever technology. In *2018 40th Annual International Conference of the IEEE Engineering in Medicine and Biology Society (EMBC)*, 4488–4491. ISSN: 1558-4615.

Lenk, C., Seeber, L., Ziegler, M., Hövel, P., and Gutschmidt, S. (2020). Enabling Adaptive and Enhanced Acoustic Sensing using Nonlinear Dynamics. In *2020 IEEE International Symposium on Circuits and Systems (ISCAS)*, 1–4. ISSN: 2158-1525.

Marsden, J.E. and McCracken, M. (1976). *The Hopf bifurcation and its applications*. Number v. 19 in Applied mathematical sciences. Springer-Verlag, New York.

Roeser, D., Gutschmidt, S., Sattel, T., and Rangelow, I.W. (2016). Tip Motion—Sensor Signal Relation for a Composite SPM/SPL Cantilever. *Journal of Microelectromechanical Systems*, 25(1), 78–90. Conference Name: Journal of Microelectromechanical Systems.

Sanders, S. and Noworolski, J. (1991). Generalized in-place circuit averaging. *EEE-PESC Rec*, 445–451.

Sanders, S., Noworolski, J., Liu, X., and Verghese, G. (1991). Generalized averaging method for power conversion circuits. *IEEE Transactions on Power Electronics*, 6(2), 251–259. Conference Name: IEEE Transactions on Power Electronics.

Slotine, J.J.E., Li, W., et al. (1991). *Applied nonlinear control*, volume 199. Prentice hall Englewood Cliffs, NJ.

Zawawi, S.A., Hamzah, A.A., Majlis, B.Y., and Mohd-Yasin, F. (2020). A review of mems capacitive microphones. *Micromachines*, 11(5), 484.